Electrochemical Formation and Characterization of Copolymers Based on *N*-Pyrrole Derivatives

Regina Okner,[†,‡] Abraham J. Domb,[†] and Daniel Mandler*[,‡]

Department of Medicinal Chemistry and Natural Products, School of Pharmacy, Faculty of Medicine, The Hebrew University of Jerusalem, Jerusalem 91120, Israel, and Department of Inorganic and Analytical Chemistry, The Hebrew University of Jerusalem, Jerusalem 91904, Israel

Received April 30, 2007; Revised Manuscript Received June 4, 2007

Organic coatings based on *N*-(2-carboxyethyl)pyrrole (PPA) and a butyl ester of PPA (BuOPy) were deposited via electrochemical oxidation. The homo- and copolymers were electropolymerized on glassy carbon and stainless steel in acetonitrile using tetrabutylammonium tetrafluoraborate (Bu_4NF_4B) as the electrolyte. The mechanism of deposition on stainless steel was studied by chronoamperometry and by the tapping and phase angle imaging modes of atomic force microscopy. The electrochemical properties and growth of the films were investigated by cyclic voltammetry. The composition of the copolymers was determined by reflection−absorption Fourier transform infrared spectroscopy. We found that while the hydrophilic monomer PPA undergoes progressive nucleation followed by instantaneous growth the hydrophobic BuOPy nucleates instantaneously. The rate of BuOPy electropolymerization was higher than that of PPA, and the resulting film was thicker yet fluffier. Copolymer films were enriched by BuOPy as compared with the electropolymerization solution, which is attributed to the faster rate of electropolymerization of BuOPy than PPA.

Introduction

Organic conducting polymers such as polypyrrole, polyaniline, and polythiophene have attracted substantial interest in recent years due to their electrochemical properties, ease of preparation, and wide range of applications.[1] They show major promise in areas such as ion exchange, batteries,[2,3] biosensors,[4−6] and corrosion inhibition.[7] Polypyrrole, for example, has been used in the preparation of polypyrrole−hyaluronic acid composite biomaterials for tissue engineering.[8] Numerous studies have been carried out aiming to investigate the different properties of conducting polymers focusing on the electrical properties.[9−11] A number of investigations have targeted the copolymerization of heterocyclic compounds of different types, such as aniline−pyrrole,[12,13] aniline−thiophene,[14] and thiophene−pyrrole.[15] The aim of these studies has been to correlate between the composition of the copolymerized mixture and the final electrochemical, physical, and morphological properties of the copolymer. Among conducting polymers, polypyrrole is by far the most studied and applied, due to its relatively low oxidation potential, high stability, and excellent electrical properties.[16]

Another approach that has been pursued as a means of controlling the properties of conducting polymers involved the synthesis and polymerization of substituted monomers. Pyrroles can easily be modified in their N position through alkylation. Such modification still allows its electropolymerization and at the same time makes it possible to modify drastically the polymer physical and chemical properties based on the characteristics of the substituents. Hence, we find it very appealing to tailor the properties of polypyrroles based on the combination of two approaches, namely, modification of the pyrrole and copolymerization.

Diaz and co-workers have studied the electrochemical behavior of N-substituted pyrrole with different functional groups and substituent size in the early 1980s.[17,18] Since then, a variety of novel N-substituted pyrroles have been synthesized and electropolymerized by varying the electrochemical conditions, electrolyte, and nature of the electrode surface.[19−21] Several research groups have focused on copolymerization of pyrrole and N-substituted pyrroles by chemical oxidation.[22−24] Yet, only a few studies have been reported on the copolymerization of N-substituted pyrroles by electrochemical oxidation. Chen-Yang et al.[25] copolymerized pyrrole with *N*-hydroxyalkyl pyrrole and characterized the resulting copolymer, which was electrodeposited on stainless steel. They noticed a different deposition mechanism for both components and discussed the influence of the functional hydroxyl groups. The researchers claimed that the electropolymerization of only *N*-hydroxyalkyl pyrrole resulted in a more condensed film than the pyrrole due to hydrogen bonding. These films showed low electroactivity in comparison with pure polypyrrole film.

Polypyrrole and its derivatives have shown potential applications in medicine due to their electrical properties, environmental and chemical stability, as well as their biocompatibility.[26,27] Such coating is essential to reduce unwanted immune response toward the bare device surface (usually metal). Hence, the coating of the device should be biocompatible and heamocompatible. Moreover, the coating of the medical device could be used also for drug elution. In a parallel study[28] we have been investigating the interaction of a polypyrrole derivative with paclitaxel (Taxol), known as a very hydrophobic drug. We found that a hydrophobic matrix is superior in maintaining the drug inside the polymer. A study describing the synthesis and electropolymerization of pyrrole-based monomers with different alkyl chains has been recently reported by us.[29] We have also examined the formation of an electrodeposited coating of polypyrrole with chemically attached poly(lactic acid) nanoparticles.[30]

* Author to whom correspondence should be addressed. Phone: +972-2-658-5831. Fax: +972-2-658-5319. E-mail: mandler@vms.huji.ac.il.
† Department of Medicinal Chemistry and Natural Products.
‡ Department of Inorganic and Analytical Chemistry.

10.1021/bm7004752 CCC: $37.00 © 2007 American Chemical Society
Published on Web 08/04/2007

Scheme 1. Chemical Structures of *N*-(2-Carboxyethyl)pyrrole (PPA) and a Butyl Ester of PPA (BuOPy)

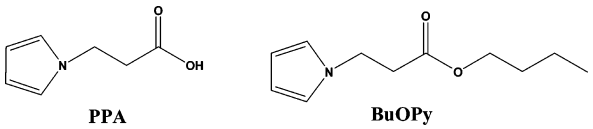

Here we report on the structure analysis and properties of copolymers based on pyrrole derivatives. Two pyrrole derivatives were examined, *N*-(2-carboxyethyl)pyrrole (PPA) and a butyl ester of PPA (BuOPy) (Scheme 1). The electrochemistry was carried out using stainless steel and glassy carbon working electrodes; the homo- and copolymers were analyzed by cyclic voltammetry and chronoamperometry. The films were analyzed by reflection−absorption Fourier transform infrared (RA-FTIR) spectroscopy, atomic force microscopy (AFM), and contact angle measurements.

Experimental Section

Materials. *N*-(2-Carboxyethyl)pyrrole (PPA) and a butyl ester of PPA (BuOPy) were synthesized as previously described.[28] The products were distilled and kept under nitrogen prior to use. Acetonitrile (ACN) (BioLab, Jerusalem, Israel), tetrabutylammonium tetrafluoraborate (Bu_4NF_4B) (Aldrich), tetrapropylammonium perchlorate (Pr_4NClO_4), and sodium perchlorate ($NaClO_4$) were used as received.

Instrumentation. Electrochemical measurements were conducted with a 630B electrochemical analyzer (CH Instruments, Austin, TX) using a three-electrode cell with Ag/AgBr as a reference electrode and a Pt wire as a counter electrode. The working electrodes were of three types: 3 mm diameter glassy carbon (GC) disks, 316L stainless steel plates, and 3 mm disks (embedded in a Teflon sheath) and thin film gold vapor deposited glass plates.

External RA-FTIR spectra were recorded using an Equinox 55 (Bruker) spectrometer equipped with a nitrogen-cooled mercury cadmium telluride detector at a resolution of 2 cm^{-1}. The spectra were acquired with a grazing angle accessory having an incident angle of 80° to the normal and a p-polarized beam. Typically, 500 scans were collected versus a reference, which was a bare gold surface.

Contact angles were measured with a Ramé-Hart model 100 contact angle goniometer. These measurements were repeated three times for each sample, and the average values are reported. All aqueous solutions were prepared from deionized water (Barnstead Easypure UV system). Thicknesses of the polymer coatings were detected by profilometery (P-15, KLA-Tencor Co., San Jose, CA). AFM measurements were conducted using a Nanoscope Dimension 3100 scanning probe microscope with a Nanoscope IVa controller.

Methods. Polypyrrole derivatives were deposited on the electrode surface using cyclic voltammetry (CV) from an ACN solution containing 0.1 M Bu_4NF_4B and 5 mM total concentration of the monomers. A potential sweep (three scans) was applied between −0.4 and 1.4 V vs Ag/AgBr at a scan rate of 0.05 V s^{-1}. The coated surfaces were rinsed with pure acetonitrile and dried with a gentle stream of nitrogen. Stainless steel plates were used for AFM, profilometry, and contact angle measurements, where the polymers were deposited by applying a constant potential (which will be detailed below) up to 60 s. Polymer films for RA-FTIR spectroscopy measurements were deposited on gold by CV.

Results and Discussion

Cyclic Voltammetry of the Pyrrole Derivatives. Figure 1 shows the cyclic voltammograms of solutions consisting of BuOPy (1), PPA (2), and a 1:1 (mole ratio) mixture of both (3) monomers using glassy carbon (GC, Figure 1A) and 316L stainless steel (SS, Figure 1B) disk electrodes.

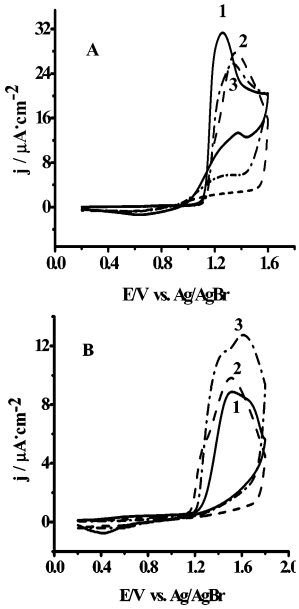

Figure 1. First cyclic voltammograms of 5 mM of BuOPy (1), PPA (2), BuOPy/PPA (bulk ratio 1:1) (3) in 0.1 M Bu_4NF_4B in acetonitrile at a scan rate of 0.05 V/s (*E* vs Ag/AgBr) recorded with glassy carbon (A) and stainless steel (B) disk electrodes.

It can be seen that both monomers as well as their mixture exhibit oxidation waves at potentials more positive than 1.2 V. Yet, the oxidation waves are less well-defined and shifted anodically on SS, which is presumably due to sluggish kinetics. In general, such organic hydrophobic compounds display facile kinetics on carbonaceous materials. The oxidation waves are substantially more positive than pyrrole as is expected due to steric and electronic factors. It has been reported that the nature of the N-substituent influences the electrochemical behavior of the monomer, but the major, i.e., steric, effect is caused by the size of the substituent.[18] We cannot determine the major factor that causes BuOPy to be oxidized at a slightly more negative potential than PPA on GC; however, we suggest that the more hydrophobic nature of the ester derivative enhances electron transfer on this hydrophobic surface. It can be seen that the oxidation wave of the mixture falls between those of the individual monomers. However, the potential difference between the individual peaks is insufficient to decide (from this measurement) whether polymerization of the mixture proceeds through real copolymerization or the wave is a superposition of the individual monomers. The cyclic voltammograms obtained on SS are difficult to interpret and will be treated differently, namely, by chronoamperometry.

Figure 2 shows the CV of the first three cycles of BuOPy (Figure 2A), PPA (Figure 2B), and their 1:1 mixture (Figure 2C). It is evident that the oxidation wave potentials do not change significantly in the course of polymerization. Furthermore, an additional oxidation wave (shoulder) appears in the second cycle and at more negative potentials for PPA and a 1:1 mixture of BuOPy and PPA. A similar behavior was observed in the electropolymerization of *N*-(*β*-hydroxy)ethylpyrrole.[19] This wave is probably associated with the negatively charged functionality of the monomer. Finally, the growth of the polymers is demonstrated by the continuous increase of the doping and undoping waves that appear at approximately 0.82 V. The increase of the currents can be correlated with the thickness of the films that was measured by profilometry. The

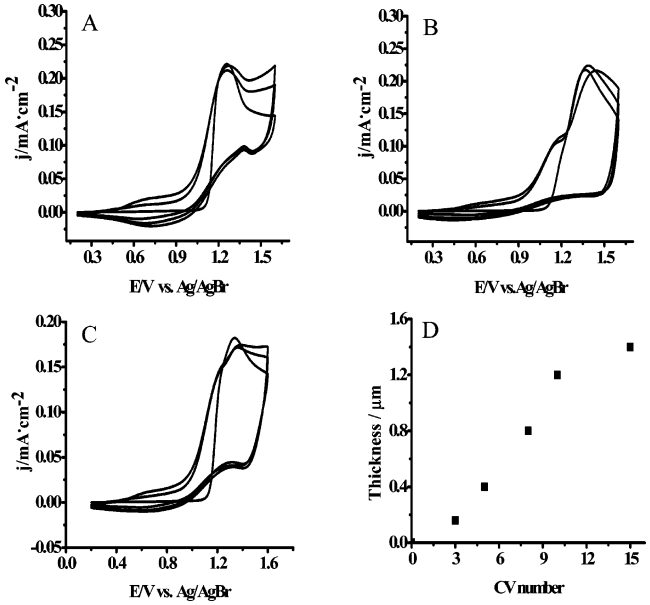

Figure 2. Cyclic voltammogram of 5 mM BuOPy (A), PPA (B), and BuOPy/PPA (bulk ratio 1:1) (C) in 0.1 M Bu_4NF_4B in acetonitrile at a scan rate of 0.05 V/s (*E* vs Ag/AgBr) recorded with a glassy carbon disk electrode. (D) pPPA film thickness dependence on number of CV cycles.

Table 1. Summary of Water Contact Angle and the Thickness of pBuOPy, pPPA, and p(BuOPy:PPA) (bulk Ratio 1:1)[a]

monomer	contact angle (deg)	thickness (μm)
BuOPy	90	1.44
PPA	35	0.41
BuOPy/PPA 1:1	78	0.93

[a] The films were deposited using chronoamperomery at a constant potential of 1.4 V up to the same charge of 0.4 Coulomb. (The deposition solution consisted of 5 mM of the monomer and 0.1 M Bu_4NF_4B in ACN.)

thickness of the polymers varies linearly with the number of cycles (Figure 2 D) up to approximately 10 cycles, which exceeds 1.2 μm.

Table 1 summarizes the water contact angle and the thickness of the polymers deposited potentiostatically on stainless steel plates. We did not observe any significant difference between deposition the films by sweeping the potential (cyclic voltammetry) or holding it at a constant value (potentiostatlically). As expected, the largest contact angle is obtained for pBuOPy due primarily to its hydrophobic nature. Yet, the contact angle depends also on the morphology as will be discussed later. The thickness of pBuOPy is also the largest as compared with pPPA and the 1:1 mixture of them, although special attention was paid to deposit the films up to the same charge (0.4 Coulomb). The contact angle and the thickness of the 1:1 copolymer lie well between the homopolymers.

The electrodeposited film can be characterized by the doping/undoping process, which is associated with the ingress and egress of usually anions. The redox potential of the system is defined as the mean of anodic and cathodic maxima. Figure 3 shows this doping/undoping process in an ACN monomer-free solution after depositing the films (three scans) on GC and SS. The electrolyte was Bu_4BF_4. It is clear that while the doping/undoping process is reversible on GC (Figure 3A) there is a substantial peak potential difference between the cathodic and anodic waves on SS (Figure 3B), which means that the doping/undoping process is significantly less reversible on stainless steel. Furthermore, the doping/undoping reversibility of pPPA

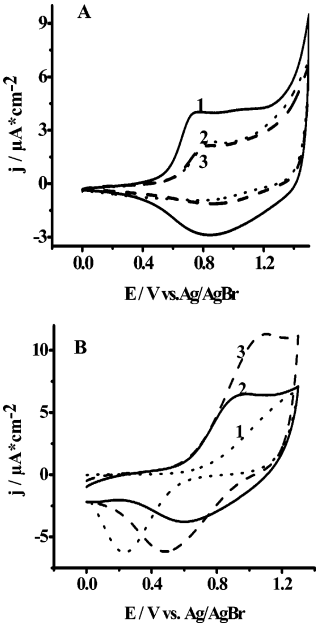

Figure 3. Cyclic voltammogram of pBuOPy/F_4B^- (1), pPPA/F_4B^- (2), p(BuOPy:PPA)/F_4B^- (bulk ratio 1:1) (3) in 0.1 M Bu_4NF_4B in acetonitrile at a scan rate of 0.05 V/s (*E* vs Ag/AgBr) on glassy carbon (A) and stainless steel (B) disk electrode.

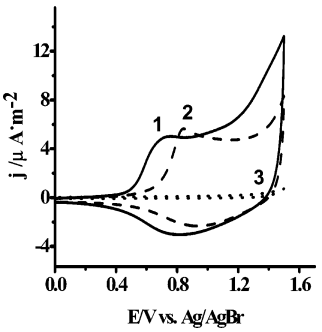

Figure 4. Cyclic voltammogram of pBuOPy/F_4B^- in acetonitrile also containing 0.1 M of the following Bu_4N^+ salts, F_4B^- (1) and ClO_4^- (2) (*E* vs Ag/AgBr), and in 0.1 M aqueous solution of ClO_4^- (3) (*E* vs Ag/AgCl).

and the copolymer on stainless steel is higher than that of pBuOPy, which is understandable taking into account the hydrophilic nature of the substrate.

Figure 4 shows the solvent and electrolyte effect on the doping/undoping waves of pBuOPy. Changing the solvent from ACN to water has a major effect and results in almost blocking this process. However, exchanging the anions (from BF_4^- into ClO_4^-) in ACN has only a minor effect on the cyclic voltammogram. It should be mentioned that the currents of the doping/undoping process in ACN for the three polymers vary linearly (R^2 equals 0.998, 0.979, and 0.997 for pBuOpy, pPPA, and p(BuOPy:PPA), respectively) with the scan rate indicating that the ingress and egress of the ion is fast independent of the film thickness.

Infrared Spectroscopy. Figure 5 shows the RA-FTIR spectra of the homopolymers pPPA and pBuOPy and copolymers formed from different bulk ratios (3:7, 1:1, and 7:3).

All spectra were normalized just for comparison. All samples were prepared by cyclic voltammetry. Each homopolymer has its typical absorbance assigned to the carbonyl band at a different wavenumber. pPPA has a broad peak at 1704 cm^{-1} (Figure 5(1)) as a result of hydrogen bonding between carboxylic units within the polymer. However, the carbonyl of the ester group of

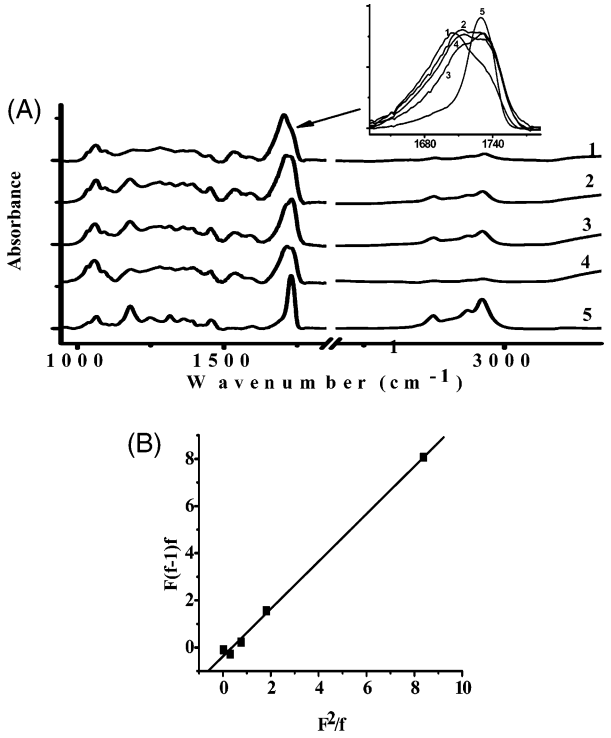

Figure 5. (A) Infrared spectra of pPPA (1), p(BuOPy:PPA) (bulk ratios of 1:1 (2), 7:3 (3), and 3:7 (4)), and pBuOPy (5) formed on stainless steel plates using CV. The inset shows the expanded spectrum of the carbonyl region. (B) Fineman−Ross plot for electrocopolymerzation of BuOPy with PPA.

Table 2. Monomer Ratios in Solution and Copolymer Composition Ratios Obtained from FTIR Curve Fitting by Integration

BuOPy/PPA (*F*) bulk ration	BuOPy/PPA (*f*) polymer composition
9:1	9.66:1
2.3:1	3:1
1:1	1.3:1
0.42:1	0.61:1
0.11:1	0.54:1

pBuOPy absorbs at 1729 cm^{-1} (Figure 5(5)). Due to this frequency difference we can easily analyze the polymer bulk composition. Figure 5 shows the IR spectra of the various compositions. It is evident that the chemical composition of the film is strongly affected by the ratio of the monomers in the electropolymerizing solution. For a 1:1 bulk ratio a double peak of the same height is obtained (Figure 5(2)), whereas for a 7:3 pBuOPy/pPPA bulk ratio a carbonyl peak consisting of two maxima (Figure 5(3)) can be detected, where the intensity of the peak corresponding to the ester is larger. The reverse picture is obtained for an opposite ratio of the monomers (Figure 5(4)). The copolymer spectra were analyzed using a curve-fitting tool, and the copolymer film's composition was evaluated by integrating the fitted peaks. The results are presented in Table 2. It can be seen that the copolymer films are enriched by the BuOPy monomer as compared to the electropolymerization solution. Nevertheless, these results do not provide accurate information about the ratio between the two structural units in the copolymer but their total ratio in the film. This is obviously due to the fact that we lack information about the molecular weight of the copolymers.

These findings are in complete agreement with our electrochemical measurements, which clearly showed that BuOPy polymerizes faster than PPA. Using the ratio of the monomers in solution and copolymer composition ratio obtained from the carbonyl FTIR peak integration, the reactivity ratios r_1 and r_2, for the monomer pair BuOPy (M_1) and PPA (M_2), can be evaluated by the Fineman−Ross[31] method, as determined by eq 1

$$F(f-1)/f = r_1(F^2/f) - r_2 \quad (1)$$

where

$$f = d[M_1]/d[M_2], \text{ copolymer composition ratio}$$

$$F = [M_1]/[M_2], \text{ monomer bulk ratio}$$

The linear plot of $F(f-1)/f = r_1(F^2/f) - r_2$ is shown in Figure 5A and yields the monomer reactivity ratios $r_1 = 1.01 \pm 0.03$ and $r_2 = 0.38 \pm 0.12$ for BuOPy and PPA, respectively. These values imply that BuOPy is 2.5 times more reactive than PPA.

Electrodeposition Process. Detailed information about the initial electrodeposition process can be extracted from chronoamperometry. Figure 6A shows the current−time ($I-t$) transients of pBuOPy (1), pBuOPy/pPPA (1:1) (2), pBuOPy/pPPA (9:1) (3), and pPPA (4) recorded during early steps of electrodeposition (up to 20 s) on a stainless steel disc electrode at a constant potential of −1.4 V. The two homopolymers pBuOPy (1) and pPPA (4) show a distinct difference during deposition on stainless steel. pBuOPy exhibits a current maximum, i_m, at longer times, t_m, as compared with pPPA, which shows a steeper current peak at shorter times.

The shapes of the recorded transients can be explained in terms of a nucleation and growth mechanism.[32] Three distinct regions can be seen in each curve. The first, where the current decreases, refers to the double-layer charging process, which is detected also during electrolysis in a monomer-free electrolyte solution.[33] The second region comprises the current maximum, which is related to the nuclei overlapping. The last region is characterized by a slow current decline that approaches a plateau. In certain cases, a second maximum is observed.[33] The charging current region is identical for all samples and will not be further discussed. The mechanism of deposition can be evaluated mainly from the second region, where the shape of the transient and the different parameters, i_m and t_m, disclose the nature of the deposition mechanism. In essence, the mechanism can be categorized into four major groups, which are expressed by the following equations:[32]

two-dimensional progressive

$$I/I_{max} = (t/t_{max}) \exp\{-2/3(t^3 - t_{max}^3)/t_{max}^3\} \quad (2)$$

two-dimensional instantaneous

$$I/I_{max} = (t/t_{max}) \exp\{-1/2(t^2 - t_{max}^2)/t_{max}^2\} \quad (3)$$

three-dimensional progressive

$$(I/I_{max})^2 = 1.2254/(t/t_{max})\{1 - \exp[-2.3367(t/t_{max})^2]\}^2 \quad (4)$$

three-dimensional instantaneous

$$(I/I_{max})^2 = 1.9542/(t/t_{max})\{1 - \exp[-1.2564(t/t_{max})]\}^2 \quad (5)$$

The pPPA transient (Figure 6A(4)) shows a rapid increase of the current within a relatively short period of time and a very clear narrow current−time shape. This can be ascribed to a progressive nucleation mechanism in which the rate of nucleation is much faster than the rate of nuclei growth. Indeed, the first part of the transient can be reasonably fit (especially at the

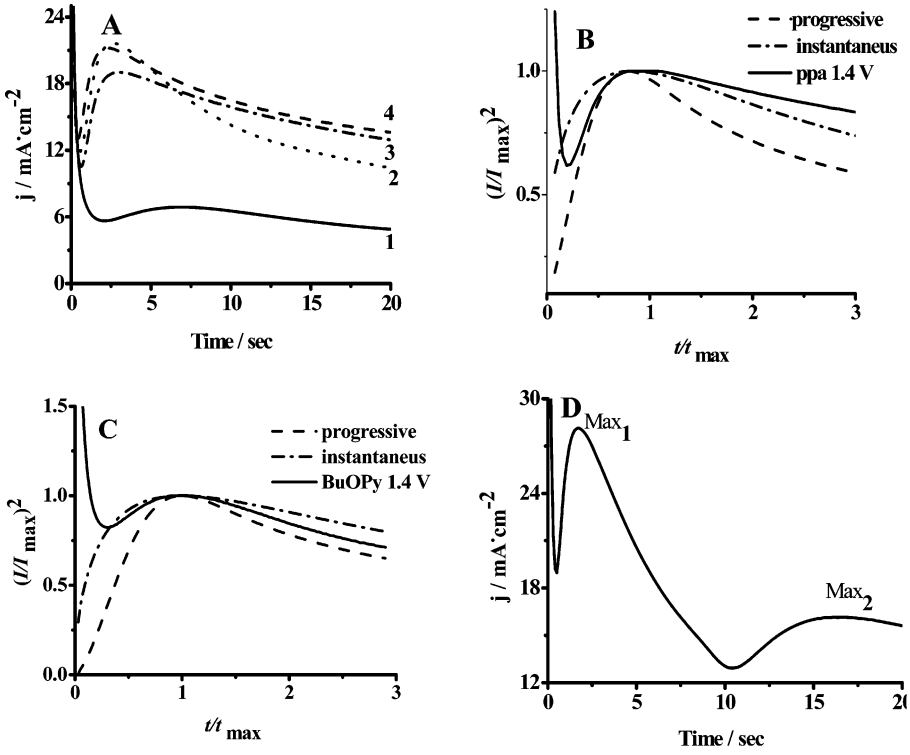

Figure 6. (A) Current−time transients (at 1.4 V) for the electrodeposition of pBuOpy(1), p(BuOpy:PPA) (bulk ratio 1:1) (2), p(BuOpy:PPA) (bulk ratio 9:1) (3), and pPPA (4) on a stainless steel disk electrode. (B and C) Dimensionless plot of current maximum vs time maximum of PPA and BuOPy deposition (Figure 6A(4 and 1)), respectively, and theoretical curves for three-dimensional instantaneous and progressive nucleation. (D) Current−time transient (at 1.6 V) for the electrodeposition of p(BuOpy:PPA) (bulk ratio 9:1) on a stainless steel disk electrode.

nucleation region) with the theoretical current−time curve (Figure 6B), whereas the decay of the current is somewhat in between the two mechanisms, implying a mixed growth mechanism. The progressive nucleation transient of pPPA reflects the fast nucleation (increase of current) that is followed by relatively slow nuclei growth until they fully overlap (current maximum) and cover the entire electrode.

However, the chronoamperometry of pBuOPy deposition (Figure 6A(1)) shows that the current reaches a maximum after a longer period of time and its intensity is somewhat lower than that of pPPA. This is explained by the number of nuclei, which is kept almost constant from the very beginning of the process. Their radii grow until nuclei overlap and cover the surface. The transient curve fits in the beginning an instantaneous nucleation process, while its decay is even more moderate than the theoretical instantaneous process (Figure 6C).

The difference between the chronoamperometry of both polymers can be explained by differences in polymer−metal interactions. Since the stainless steel surface is covered with a thin oxide layer, which is hydrophilic to some extent (contact angle 60°), it is likely to better interact with hydrophilic and polar species, such as PPA. This interaction favors the progressive nucleation. Alternatively, hydrophobic species, which do not interact strongly with the interface, will deposit via the instantaneous nucleation mechanism, where nuclei growth dominates over nucleation.

Inspecting the current−time transients of mixtures of monomers reveals interesting, however, expected behavior. Namely, the addition of even relatively small amounts of PPA (10%) (in p(BuOPy:PPA) (9:1)) into a solution of BuOPy changes the mechanism of polymerization from instantaneous to progressive deposition. This can be accounted for by the preferred interactions of PPA with the SS surface, which results in the favorable initial deposition of pPPA. Thus, we expect that the very initial film will be enriched with pPPA, which serves as a suitable (more hydrophobic) substrate for further deposition of pBuOPy. Indeed, electrodeposition of BuOPy/PPA (9:1) at a high potential (1.6 V) gives two well-defined maxima, Max_1 and Max_2 (Figure 6D). Hence, the chronoamperometry results are in accordance

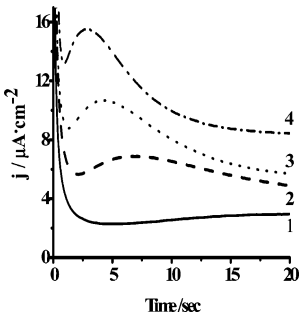

Figure 7. Current−time transients for the electrodeposition of pBuopy on a stainless steel disk electrode. Potential steps of 1.3 (1), 1.4 (2), 1.5 (3), and 1.6V (4) vs Ag/AgBr.

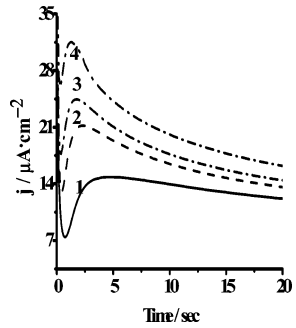

Figure 8. Current−time transients for the electrodeposition of pPPA on a stainless steel disk electrode. Potential steps are the same as in Figure 7.

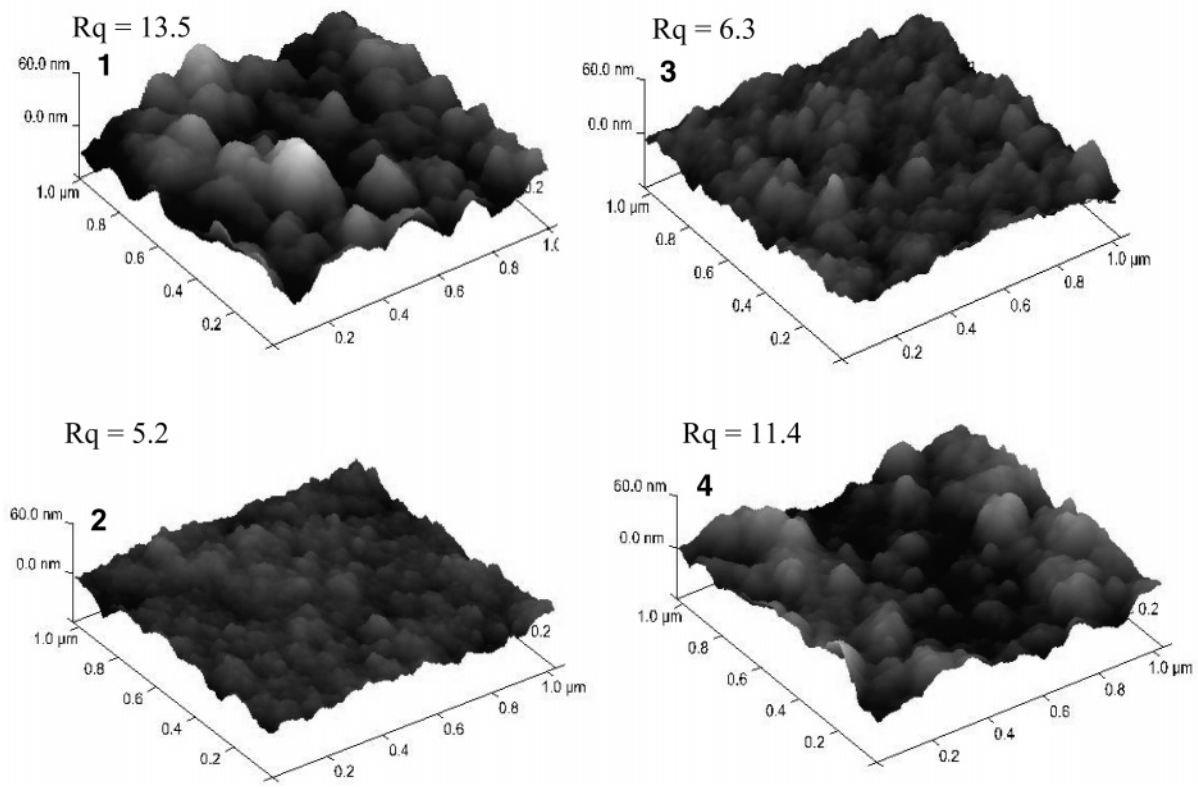

Figure 9. Three-dimensional AFM images of pBuOPy (1), pPPA (2), p(BuOPy:PPA) (bulk ratio 1:1) (3), and p(BuOPy:PPA) (bulk ratio 9:1) (4) formed on stainless steel plates using chronoamperometry (potential of deposition equals 1.4 V vs Ag/AgBr). Roughness parameters (Rq) are added for each image.

with the FTIR findings described above that show that the final bulk deposition is enriched with hydrophobic pBuOPy.

The mechanism of deposition of each polymer can be altered by the applied potential. Figures 7 and 8 show the effect of the applied potential on the transients of pBuOPy and pPPA, respectively. It can be seen that the chronoamperometry of pBuOPy changes drastically as the applied potential varies from 1.3 to 1.6 V. As the driving force for deposition increases, the shape of the transient matches better a progressive nucleation. This is understandable and in agreement with previous reports.[34] Polymerization of pPPA, which proceeds even at lower overpotentials via progressive nucleation, does not change dramatically; moreover, it fits better with the progressive mechanism.

AFM Analysis. AFM imaging was used for supporting our chronoamperometry findings and correlate between the transients and surface morphology and composition. AFM in its different modes of operation, e.g., tapping and phase imaging modes, can provide invaluable information about polymer roughness and composition.[35] Figure 9 represents AFM height images of pBuOPy(1), pPPA (2), p(BuOPy:PPA) (bulk ratio 1:1) (3), and p(BuOPy:PPA) (bulk ratio 9:1) (4) formed by chronoamperometry (60 s) at 1.4 V. We anticipated that progressive nucleation would result in smoother films than polymers formed via instantaneous nucleation. This has already been reported for different conducting polymers.[36−39] Indeed, inspecting the AFM images and the data in Table 1 (contact angle values difference) clearly shows that a pPPa film is smoother than a pBuOPy film. The copolymers give surface morphologies that are in accordance with their bulk ratios.

As we look at AFM height images of p(BuOPy:PPA) (bulk ratio 9:1) (4) it can be seen that its roughness parameters are more close to those of pBuOPy, in contrast with the current−time transient curve, which was more similar to pPPA (Figure 6). This can be explained by changing the deposition mechanism after nuclei overlapping.[37] Namely, whereas before nuclei overlapping PPA was predominantly deposited, the film grows with a similar composition of the solution after the pristine surface is entirely covered by a polymer.

To obtain information about the local distribution of the different monomer units inside the film, we have used phase imaging AFM (Figures 10A′−D′). This technique, which is based on mapping the phase of the cantilever oscillation during the tapping mode scan, provides important information beyond simple topographical mapping (Figures 10A−D) that allows the detection of variations in composition, viscoelasticity, friction, and other properties.[35] This application makes it possible to identify contaminants and map different components in composite materials at very high resolution, which cannot be achieved by the tapping mode. The composition difference of the films is clearly revealed by contrast changes in phase imaging.

Figure 10 shows the phase imaging of electropolymerized films made of pBuOPy (A′), pPPA (B′), p(BuOPy:PPA) (bulk ratio 1:1) (C′), and p(BuOPy:PPA) (bulk ratio 9:1) (D′). It can be seen that there are no contrast changes indicating that the films are made of homopolymers. A distinct difference is disclosed upon imaging the copolymers. The phase imaging of a sample made of 1:1 p(BuOPy:PPA) shows a clear contrast between the two components, which are homogeneously distributed across the surface. The phase imaging of the copolymer composed of 9:1 p(BuOPy:PPA) also shows a clear contrast between the components constituting the surface, however, to a lesser extent than the 1:1 copolymer. This is in complete agreement with our FTIR results discussed above.

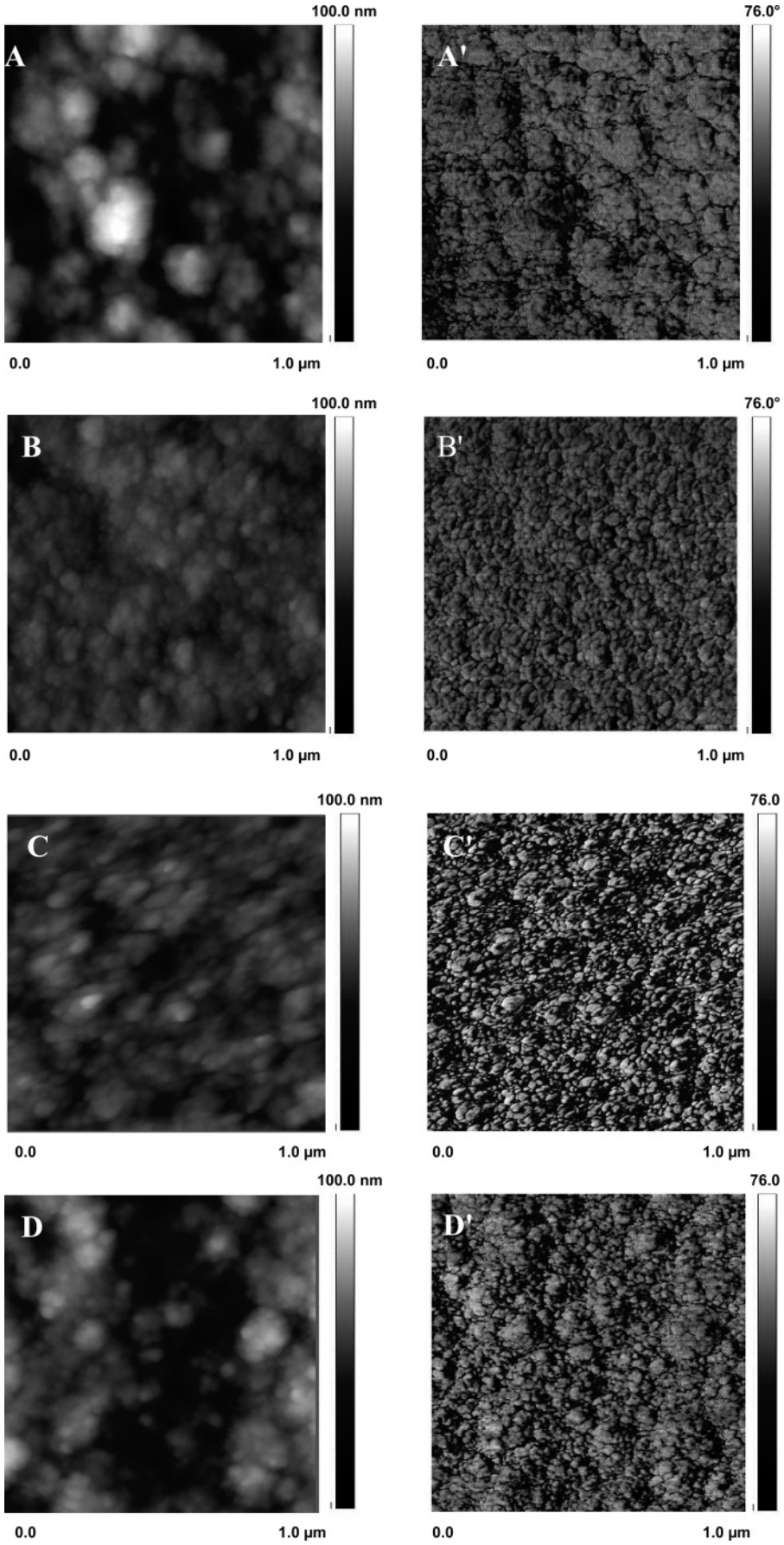

Figure 10. Tapping mode (left) and phase (right) images of a pBuOPy (A), pPPA (B), p(BuOPy:PPA) (bulk ratio 1:1) (C), and p(BuOPy:PPA) (bulk ratio 9:1) (D).

Conclusions

A series of *N*-(2-carboxyethyl)pyrrole (PPA) and a butyl ester of PPA (BuOPy) copolymers and their corresponding homopolymers were electrochemically deposited on glassy carbon and stainless steel surfaces. It has been shown that the structural features of these two monomers resulted in different deposition mechanisms and electrochemical and physical properties of the polymer films. Changing the monomer solution ratio and deposition conditions also allowed us to create structurally, chemically, and electrically different polymer films, which may provide opportunities for a broad spectrum of medical applications such as implantable device coatings for drug elution.

Acknowledgment. This work was supported by the Hebrew University through an applied grant and by Elutex. The unit for nanocharacterization of the Hebrew University is acknowledged. This work was supported in part by a grant from the Israel Science Foundation.

References and Notes

(1) Skotheim, T. A. *Handbook of Conducting Polymers*; Marcel Dekker: New York, 1986; Vol 1.
(2) Li, F. B.; Albery, W. J. *J. Electroanal. Chem.* **1991**, *302*, 279−284.
(3) Novak, P.; Muller, K.; Santhanam, K. S. V.; Haas, O. *Chem. Rev.* **1997**, *97*, 207−282.
(4) John, R.; Wallane, G. *J. Electroanal. Chem.* **1990**, *283*, 87−98.
(5) Uang, Y. M.; Chou, T. C. *Biosens. Bioelectron.* **2003**, *19*, 141−147.
(6) Jun, H. K.; Hoh, Y. S.; Lee, B. S.; Lee, S. T.; Lim, J. O.; Lee, D. D.; Huh, J. S. *Sens. Actuators, B* **2003**, *6*, 576−581.
(7) Li, P.; Tan, T. C.; Lee, J. Y. *Synth. Met.* **1997**, *88*, 237−242.
(8) Collier, J. H.; Camp, J. P.; Hudson, T. W.; Schmidt, C. E. *J. Biomed. Mater. Res.* **2000**, *50*, 574−584.
(9) Kanazawa, K. K.; Diaz, A. F.; Geiis, R. H.; Gill Kwak, J. F.; Logan, J. A.; Rabolt, J. F.; Street, G. B. *J. Chem. Soc., Chem. Commun.* **1979**, *19*, 854−855.
(10) Hernandez, R.; Diaz, A. F.; Waltman, R.; Bargon, J. *J. Phys. Chem.* **1984**, *88*, 3333−3337.
(11) Rajagopalan, R.; Iroh, J. O. *Electrochim. Acta* **2001**, *46*, 2443−2455.
(12) Rajagopalan, R.; Iroh, J. O. *Appl. Surf. Sci.* **2003**, *218*, 58−69.
(13) Zotti, G.; Cattarin, S.; Comisso, N. *J. Electroanal. Chem.* **1988**, *239*, 387−396.
(14) Otero, T. F.; Rodriguez, J.; Angulo, E.; Santamarias, C. *Synth. Met.* **1993**, *57*, 3713−3717.
(15) Kuwabata, S.; Ito, S.; Yoneyama H. *J. Electrochem. Soc.* **1988**, *135*, 1691−1695.
(16) Verenitskaya, T.V.; Efimov, O. N. *Russ. Chem. Rev.* **1997**, *66*, 443−57.
(17) Diaz, A. F.; Castillo, J.; Logan J. A.; Lee, W. Y. *J. Electroanal. Chem.* **1981**, *129*, 115−132.
(18) Diaz, A. F.; Castillo, J.; Kanazawa, K. K.; Logan, J. A.; Salmon, M.; Fajardo, O. *J. Electroanal. Chem.* **1982**, *133*, 233−239.
(19) Cross, M. G.; Walton, D.; Morse, N. J.; Mortimer, R. J; Rosseinsky, D. R.; Simmonds, D. J. *J. Electroanal. Chem.*, **1985**, *189*, 389−396.
(20) Haase, V.; Beck, F. *Electrochim. Acta* **1994**, *39*, 1195−1205.
(21) Tsuchiya, M.; Matsui, S.; Sano, K.; Kojima, T. *J Appl. Polym. Sci.* **1998**, *70*, 471−475.
(22) Stanke, D.; Hallensleben, M. L.; Toppare, L. *Synth. Met.* **1995**, *72*, 167−171.
(23) Ustamehmetoglu, B.; Kelleboz, E.; Sarac, A. S. *Int. J. Polym. Anal. Charact.* **2003**, *8*, 255−268.
(24) Kiskan, B.; Akar, A.; Kizilcan, N.; Ustamehmetoglu B. *J. Appl. Polym. Sci.* **2005**, *96*, 1830−1834.
(25) Chen-Yang, Y. W.; Li, J. L.; Wu, T. L.; Wang, W. S.; Hon, T. F. *Electrochim. Acta* **2004**, *49*, 2031−2040.
(26) Zang, Z.; Roy, R.; Dugre, J. F.; Tessier, D.; Dao, H. L. *J. Biomed. Mater. Res.* **2001**, *57*, 63−71.
(27) Wang, X.; Gu, X.; Yuan, C.; Chen, S.; Zhang, P.; Zhang, T.; Yao, J.; Chen, G.; Chen, F. *J. Biomed. Mater. Res., Part A* **2004**, *68*, 411−422.
(28) Okner, R.; Oron, M.; Nyska, A.; Tal, N.; Mandler, D.; Domb, A. J. Electrocoating of stainless steel coronary stents for extended release of paclitaxel. *J. Biomed. Mater. Res., Part A*, in press.
(29) Weiss, Z.; Mandler, D.; Shustak G.; Domb, A. J. *J. Polym. Sci., Part A: Polym. Chem.* **2004**, *42*, 1658−1667.
(30) Shustak, G.; Gadzinowski, M.; Slomkowski, S.; Domb, A. J.; Mandler, D. *New J. Chem.* **2007**, *1*, 163−168.
(31) Fineman, M.; Ross, S. D. *J. Polym. Sci.* **1950**, *5*, 259−262.
(32) Harrison, J. A.; Thirsk, H. R. In *Electroanalytical Chemistry*; Bard, A. J., Ed.; Academic Press: New York, 1971; Vol. 5, pp 67−103.
(33) Palomar-Pardave, M.; Miranda-Hernandez, M.; Gonzfilez, I.; Batina, N. *Surf. Sci.* **1998**, *399*, 80−95.
(34) Shustak, G.; Domb, A. J.; Mandler, D. *Langmuir* **2006**, *22*, 5237−5240.
(35) Magonov, S. N.; Elings, V.; Whangbo, M. H. *Surf. Sci.* **1997**, *375*, L385−L391.
(36) Hwang, B. J.; Santhanam, R.; Lin, Y. L. *Electroanalysis* **2003**, *15*, 115−120.
(37) Li, F. B.; Albery, W. J. *Langmuir* **1992**, *8*, 1645−1653.
(38) Bade, K.; Tsakova, V.; Schultze, J. W. *Electrochim. Acta* **1992**, *37*, 2255−2261.
(39) Asavapiriyanont, S.; Chandler, G. K.; Gunawardena, G. A.; Pletcher, D. *J. Electroanal. Chem.* **1984**, *177*, 229−244.

BM7004752